Spiral magnetic structure of Fe in Van der Waals gapped FeOCl and polyaniline-intercalated FeOCl

S. R. Hwang, W.-H. Li, and K. C. Lee
Department of Physics, National Central University, Chung-Li, Taiwan 32054, Republic of China

J. W. Lynn
NIST Center for Neutron Research, NIST, Gaithersburg, Maryland 20899-8562

C.-G. Wu
Department of Chemistry, National Central University, Chung-Li, Taiwan 32054, Republic of China
(Received 16 February 2000; revised manuscript received 21 June 2000)

High-resolution and magnetic neutron-diffraction measurements were performed to investigate the crystal and magnetic structures of bilayered FeOCl and polyaniline-intercalated FeOCl. A quasi-two-dimensional crystallographic structure, where charge neutral $(Fe_2O_2Cl_2)_n$ lamellas are weakly linked via Van der Waals interactions, has made FeOCl a good host for accommodating guest molecules. A three-dimensional long-range ordering of the Fe spins in FeOCl develops below 80 K, with a magnetic unit cell 28 times the size of the nuclear one. A spiral magnetic structure was obtained, reflecting the competition between antiferromagnetic superexchange coupling and ferromagnetic direct exchange coupling. Polyaniline intercalation interrupts the magnetic correlations between the neighboring bilayers, rendering a coupled-bilayer quasi-two-dimensional magnetic order for the Fe spins in $(C_6D_4ND)_{0.16}FeOCl$. No significant change on the ordering temperature of the Fe spins by the intercalation reaction was observed.

I. INTRODUCTION

As a promising material for practical applications in a variety of devices, electrically conductive polymers have recently received considerable attention. One way to reduce tangling in polymer molecules and to obtain orientated polymer chains is to grow them inside a structurally organized host framework, with accessible oriented tunnels. The quasi-two-dimensional (Q2D) nature, that is a result of the appearance of Van der Waals crystallographic gaps,[1] has made FeOCl an excellent inorganic host for intercalation reactions.[2] Various electrically active materials, such as tetrathiafulvalene,[3] polypyrrole,[4] and polyaniline (C_6H_4NH),[5,6] have been intercalated into FeOCl to form good low-dimensional conductors. Lithium ion intercalated FeOCl has also been used[7–9] as cathode materials for rechargeable lithium batteries. The topochemical substitution of the Cl layers in FeOCl with OH layers has been found[10–12] to help stabilize the intercalated Li^+ ions and to improve the cathode performance.

Until recently, many of the studies made on the FeOCl related compounds had concentrated on their electrochemical properties, relatively fewer on their basic properties, which remain poorly understood. Phonon spectra of FeOCl for energies below 80 meV have been reported[13] to resolve six broad vibrational modes using inelastic neutron-scattering measurements. A spiral magnetic structure, characterized by a propagation vector of (0.275 0.5 0.5), for the Fe spins in FeOCl has been proposed[14] based on neutron-diffraction measurements. In the present work, we have performed neutron-diffraction measurements to explore the detailed crystal and magnetic structures of naturally bilayered FeOCl as well as polyaniline-intercalated FeOCl. The results may provide valuable information regarding to the effects of the presence of electrically conducting guest to the magnetic properties of the host. We have found, in FeOCl, a spiral spin arrangement along the shortest crystallographic axis direction, that we believe is a direct result of the competition between the ferromagnetic Fe-Fe direct exchange coupling and the antiferromagnetic Fe-Fe superexchange coupling mediated through the O ions located between them. For spins along the other two crystallographic directions, where the strength of the Fe-O-Fe superexchange coupling was geometrically reduced, simpler spin arrangements are observed. A bilayered Q2D magnetic order was found for the Fe spins in polyaniline-intercalated FeOCl, showing that the intercalation reaction interrupts the magnetic interaction between the neighboring $(Fe_2O_2Cl_2)_n$ bilayers.

II. CRYSTAL STRUCTURE

Polycrystalline iron-oxychloride FeOCl was prepared by the chemical vapor transport technique.[15] High-purity Fe_2O_3 and $FeCl_3$ powders with a mole ratio of 1:1.3 were mixed well and then sealed in an evacuated glass tube, followed by heating at 380 °C for 40 h. They were then slowly cooled to room temperature. The resultant product was washed thoroughly with water-free acetone to remove the excess $FeCl_3$, and dried naturally in vacuum. The grains in the resultant polycrystalline sample had a lamellar, rather than spherical, shape reflecting the anisotropic crystallographic structure of the compound. FeOCl is rather sensitive to humidity, thus isolation from the atmospheric environment at all times is essential to keep the compound from being hydrated. For polyaniline-intercalated FeOCl, 100 ml of a 3% deuterated aniline solution (32.3 mmol) in acetonitrile was stirred with

5.0 g (4.66 mmol) FeOCl in air for a week. The black shiny microcrystalline product was then isolated by filtration, washed with acetone and dried naturally in vacuum. The intercalation reaction was deemed complete when the (0 0 *k*) peaks of the starting FeOCl disappeared from the x-ray powder-diffraction pattern. Elemental analysis shows a C_6D_4ND to FeOCl ratio of 0.16:1, hence a chemical formula of $(C_6D_4ND)_{0.16}FeOCl$, for the resultant product. This polyaniline intercalated FeOCl compound is hereafter denoted as $(PANI)_{0.16}FeOCl$.

X-ray-diffraction measurements were used first to characterize the sample, and the detailed crystal structure was determined by a complete structural analysis using neutron-diffraction measurements and Rietveld analysis.[16,17] A high-resolution neutron-diffraction pattern, covering a scattering-angle range from 3° to 165° and taken at room temperature, was collected on BT-1, the 32-detector powder diffractometer at the NIST Center for Neutron Research. The neutrons had a wavelength of $\lambda = 1.5401$ Å, defined by a Cu(311) monochromator crystal. Angular collimators with horizontal divergences of 15′, 20′, and 7′ full width at half maximum (FWHM) acceptances were used for the in-pile, monochromatic, and diffracted beams, respectively. During the measurements, the sample was loaded into a cylindrical vanadium can, which produces no measurable neutron-diffraction peaks, and was slowly rotating about the cylindrical axis to account for the anisotropic sharp of the grains in the sample.

The diffraction pattern was analyzed using the GSAS (General Structure Analysis System) program,[18] following the Rietveld refinement method, with coherent scattering amplitudes of 0.954, 0.580, and 0.958×10^{-12} cm for Fe, O, and Cl, respectively. Several models with different symmetries were assumed during the preliminary analysis. The refinement was finally carried out by assuming an orthorhombic symmetry of space group *Pmmn*, with a unit cell consisting of two pairs of distorted Cl-Fe-O chains. All structural and lattice parameters were allowed to vary simultaneously until R_w, the weighted *R* factor, differed by less than one part in a thousand within two successive cycles. Figure 1 shows the observed (crosses) and fitted (solid lines) patterns of FeOCl, with their differences plotted at the bottom. Clearly, the calculated and the observed patterns agree very well, showing that the observed pattern can be adequately described by the proposed structure shown in Fig. 2, which is the same one as has been proposed in other studies.[1,19,20] Table I lists the refined structural parameters and selected bond angles, which are in good agreement, but are more precise than those reported in other studies.[1,19] Uncertainties quoted here and throughout this article are statistical and represent one standard deviation. Note that the isotropic temperature parameter *B*, which indicates the mean-square displacement of the atoms from their average sites, is much larger for Cl atoms than for Fe and O atoms, showing that the Cl atoms are relatively weakly bound to the other atoms. Note that there is essentially no improvement made for refinements using anisotropic temperature parameters. Employing the Dollase and March model,[21,22] a factor of 1.57 was obtained for *c*-axis preferred orientation, accounting for the anisotropic shape of the grains in the polycrystalline sample. We estimated any impurity phases in the sample to be less than 1%.

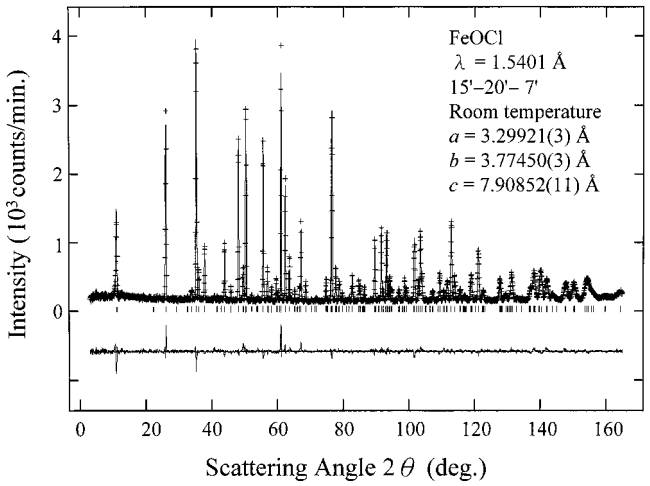

FIG. 1. Observed (crosses) and fitted (solid lines) neutron powder-diffraction patterns of FeOCl collected at room temperature. The differences are plotted at the bottom. The short vertical lines shown below the pattern mark the calculated positions of the Bragg reflections.

The crystal structure of FeOCl may be viewed as a stacking of charge-neutral Q2D $(Fe_2O_2Cl_2)_n$ lamellas, where the adjacent blocks are weakly bonded[23] via Van der Waals interactions, with a gap separation of 2.69617(3) Å at room temperature. We note that the Fe-O-Fe bond angles and the Fe-Fe separations along the three crystallographic directions are quite different, resulting in different magnetic interactions and resultant configurations for the Fe spins along the

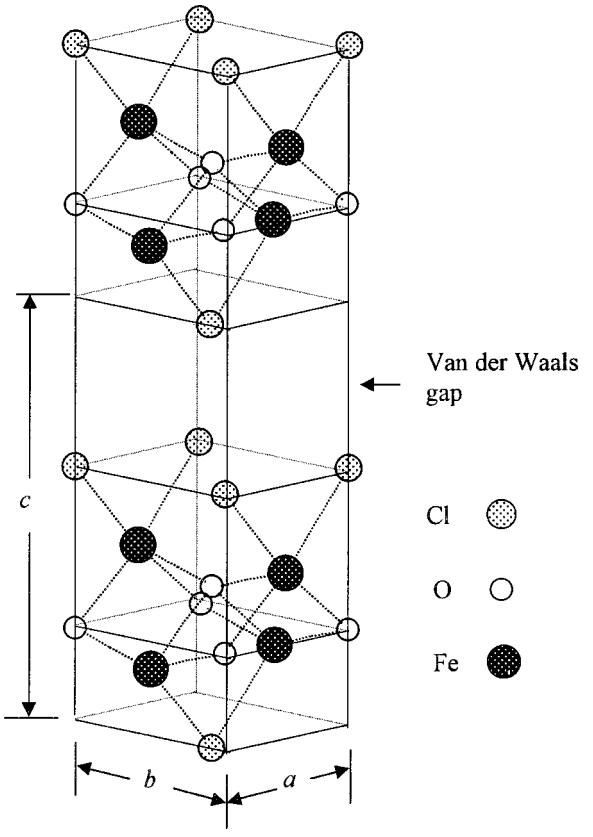

FIG. 2. Proposed crystal structure of FeOCl, where a unit cell contains two sets of distorted Cl-Fe-O chains.

TABLE I. Refined structural parameters, selected bond lengths, and bond angles for FeOCl at room temperature. B represents the isotropic temperature parameter with $B \equiv \pi^2 \langle \mu^2 \rangle$, where $\langle \mu^2 \rangle$ is the mean-square displacement.

FeOCl, space group *Pmmn*, room temperature $a = 3.29921(3)$ Å, $b = 3.77450(3)$ Å, $c = 7.90852(11)$ Å					
Atom	x	y	z	B (Å^2)	Occupancy
Fe	0.75	0.25	0.1154(1)	0.76(2)	0.99(1)
O	0.25	0.25	0.9510(2)	0.85(3)	0.99(1)
Cl	0.25	0.25	0.3301(1)	1.57(2)	1.00(1)
$R_p(\%) = 5.11$		$R_w(\%) = 6.15$		$\chi = 1.31$	
		Fe-O-Fe bond angle		Fe-Fe bond length	
Along a		103.49(4)°		3.29921(2) Å	
Along b		148.89(4)°		3.77450(3) Å	
Along c		99.56(6)°		3.10065(6) Å	

three directions (see below). Apparently, the Q2D structural nature makes FeOCl a good inorganic host[26] for accommodating guest molecules in the Van der Waals gaps, and forming intercalated FeOCl. The basic $(Fe_2O_2Cl_2)_n$ lamellas consist of edge-sharing distorted $FeCl_2O_4$ octahedrons, with the Cl layers outermost on either side of a central $(FeO)_2$ bilayer, forming a bilayered Q2D Fe-O-Fe network (designated as the a-b plane), while the network along the c-axis direction is interrupted by two weakly bonded Cl layers.

Intercalation reaction of polyaniline into FeOCl results in a 103% increase in the gap separation, apparently due to the existence of polyaniline in the Van der Waals gaps, and a shift, by an amount of $(a/2\, b/2)$, in the relative positions between the two neighboring bilayers separated by polyaniline. A 230% increase in the c axis parameter hence resulted. The lateral shift in the neighboring bilayers found for the present $(PANI)_{0.16}FeOCl$ is similar to what has been observed[3] in a tetrathiafulvalene-intercalated FeOCl. On the other hand, the crystal structure within the bilayered $(Fe_2O_2Cl_2)_n$ lamellas remains, with the a and b axis parameters both increase by $\sim$1.5%. Unfortunately, the positional parameters for polyaniline in the present compound can not be uniquely determined from the present data, mainly due to the lack of a crystalline periodicity in the polyaniline themselves.

III. MAGNETIC STRUCTURE

Neutron magnetic diffraction experiments were also conducted at NIST, using the BT-9 and BT-4 triple-axis spectrometers operated in the double-axis mode. The magnetic diffraction of FeOCl was carried out on the BT-9, whereas the BT-4 was used to collect data for $(PANI)_{0.16}FeOCl$. The neutrons used had a wavelength of $\lambda = 2.359$ Å defined by using a pyrolytic graphite PG(002) monochromator crystal. A PG filter placed before the monochromator position was employed to suppress any higher-order wavelength contamination. For the measurements performed at BT-9 (BT-4), angular collimators of horizontal divergences 40′-48′-48′ (60′-40′-40′) FWHM acceptance for the in-pile, monochromatic, and diffracted beams, respectively, were employed. During the measurements, the sample was loaded into a cylindrical aluminum can filled with helium exchange gas to facilitate thermal conduction at low temperatures. The sample was cooled using a closed-cycle refrigerator, operated between 10 and 200 K.

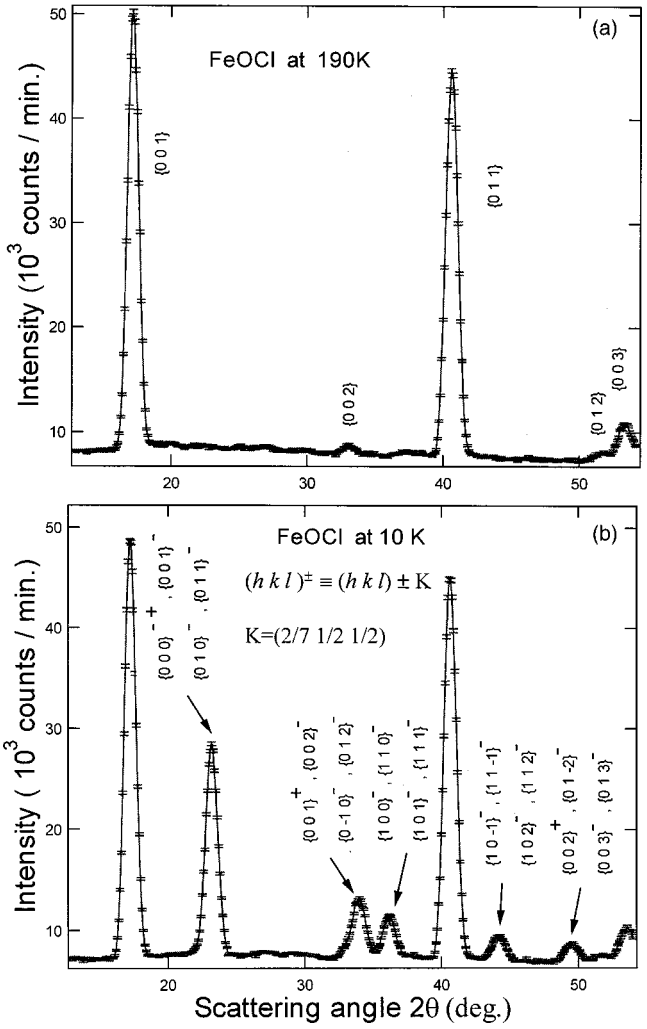

FIG. 3. Neutron-diffraction patterns of FeOCl taken at (a) 190 K and (b) 10 K. The magnetic peaks are indexed using the notation of $(h\,k\,l)^{\pm} \equiv (h\,k\,l) \pm (2/7\ 1/2\ 1/2)$.

A. FeOCl

At temperatures well above the magnetic ordering temperature, the spins of unpaired electrons scatter neutrons incoherently, so that the magnetic scattering appears as a paramagnetic background in the diffraction pattern. When magnetic order develops, at temperatures below the ordering temperature, the magnetic scattering evolves into Bragg peaks. Figures 3(a) and 3(b) show the diffraction patterns taken at 190 and 10 K, respectively. The solid curves are fits of the data to the Gaussian instrumental resolution function. All the peaks in the pattern taken at 190 K can be indexed (as shown) based on the crystallographic unit cell listed in Table I, but using somewhat smaller lattice constants due to thermal contraction. A series of new resolution-limited peaks (as indicated by the arrows) developed as the temperature was reduced to 10 K, signifying the long-range ordering of the Fe spins.

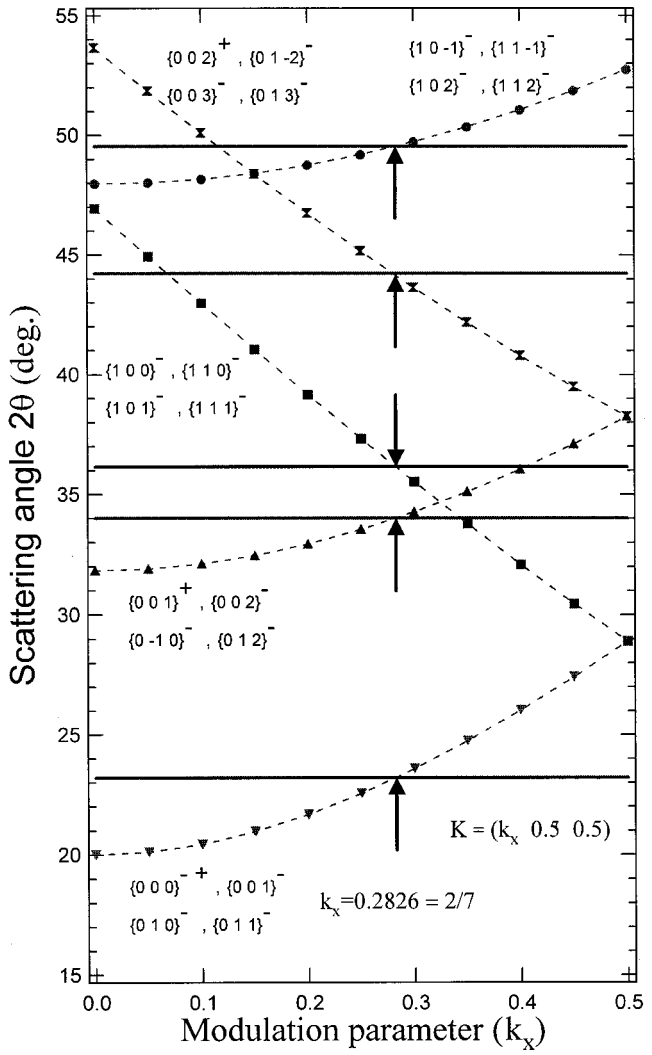

FIG. 4. The observed (solid lines) and calculated (dashed lines) Bragg angles for the propagation vectors $(h\,k\,l)^{\pm}\equiv(h\,k\,l)\pm(k_x\,1/2\,1/2)$ as a function of the modulation parameter k_x. The arrows indicate the positions where the observed and calculated lines meet.

We employed a diagrammatic method,[24] based on symmetry considerations, to find the appropriate propagation vectors, $(hkl)^{\pm}\equiv(hkl)\pm\mathbf{K}$, where $\mathbf{K}=(k_xk_yk_z)$ is the modulation vector for the magnetic peaks. The only **K** that fit the observed magnetic peaks properly is shown in Fig. 4. The horizontal solid lines represent the Bragg positions of the observed magnetic peaks and the dashed lines mark the calculated ones for a modulation vector, $\mathbf{K}=(k_x\,0.5\,0.5)$. Apparently, at $k_x=0.2826=2/7$ all five calculated lines intersect the observed ones, as indicated by the arrows. The vector (0.2826 0.5 0.5) obtained for the modulation parameters is the only one that fits the data, as is expected from the uniqueness of the irreducible representation,[24] and is essentially the same with the one reported by Adam and Buisson.[14] Accordingly, the magnetic peaks were then indexed by adopting the notation $(hkl)^{\pm}\equiv(hkl)\pm(2/7\ \ 1/2\ \ 1/2)$, as marked in Fig. 3(b). The magnetic unit cell is then double the nuclear one in both the *b* and *c* axis directions, while it is seven times longer in the *a*-axis direction. There are therefore 28 nuclear unit cells and 56 Fe ions in a magnetic unit cell.

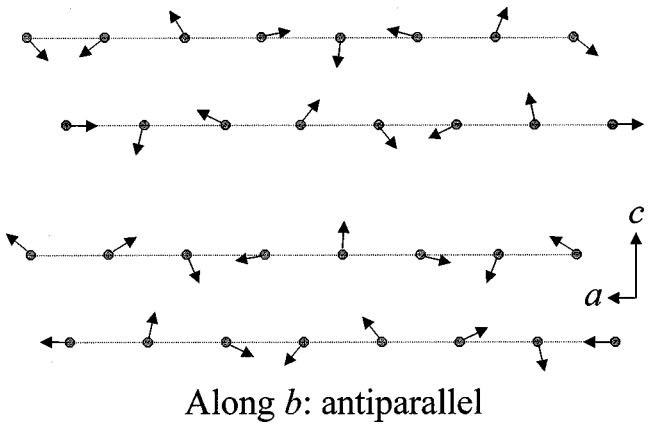

FIG. 5. Proposed magnetic structure for Fe spins in the *a*-*c* plane, showing a spiral spin arrangement along the *a*-axis direction.

It is certainly not a simple matter to determine the spin arrangement. We employed the symmetry group analysis method[25] to model the magnetic structure. The spin vectors of the Fe ions can be decomposed into a superposition of magnetic basis functions, which work as the basic magnetic configuration modes. In terms of the magnetic basis functions, the spin vector of the *j*th Fe ion in a designated basis nuclear unit cell may be expressed as

$$\mathbf{S}_{bj}=\sum C_k\mathbf{m}_k,$$

where C_k is the superposition coefficient for the magnetic basis function $\mathbf{m}_k$. The spin vector of the *j*th Fe ion in the *n*th nuclear unit cell, which can be reached from the basis unit cell by the application of a translation vector $\mathbf{R}_n$, then takes the form of

$$\mathbf{S}_{rj}=\sum \mathbf{S}_{bj}\exp(i\alpha_n),$$

where $\alpha_n=\mathbf{K}\cdot\mathbf{R}_n$ and the summation takes over the two magnetic modulation vectors $\pm\mathbf{K}$.

For a symmetry of space group *Pmmn*, there is one irreducible representation.[26] The star of **K** contains two arms for the two modulation vectors $\pm\mathbf{K}$, each of which is associated with two row vectors. There are therefore 12 magnetic basis functions for each Fe ion. We then calculated the intensity[24] for all possible combinations of the magnetic basis functions, and found that only the set of spin vectors where

TABLE II. Calculated and observed magnetic integrated intensities, where $\{h\,k\,l\}^{\pm}\equiv\{h\,k\,l\}\pm(2/7\ 1/2\ 1/2)$. The intensities are normalized with respect to the peak at 23.2°.

Peak index $\{h\,k\,l\}$	$2\theta_{obs}$	I_{obs}	I_{cal}
$\{0\,0\,0\}^{\pm}+\{0\,0\,1\}^{-}+\{0\,1\,0\}^{-}+\{0\,1\,1\}^{-}$	23.20°	1.00(1)	1
$\{0\,0\,1\}^{+}+\{0\,0\,2\}^{-}+\{0\,\bar{1}\,1\}^{+}+\{0\,1\,2\}^{-}$	34.00°	0.32(2)	0.36
$\{1\,0\,0\}^{-}+\{1\,1\,0\}^{-}+\{1\,0\,1\}^{-}+\{1\,1\,1\}^{-}$	36.15°	0.27(2)	0.27
$\{1\,0\,\bar{1}\}^{-}+\{1\,1\,\bar{1}\}^{-}+\{1\,0\,2\}^{-}+\{1\,1\,2\}^{-}$	44.19°	0.15(3)	0.18
$\{0\,0\,2\}^{+}+\{0\,1\,\bar{2}\}^{-}+\{0\,0\,3\}^{-}+\{0\,1\,3\}^{-}$	49.54°	0.11(4)	0.16

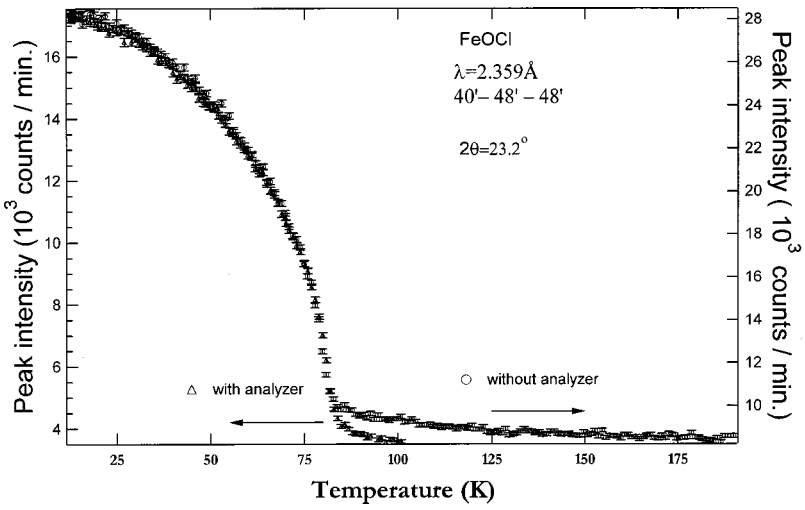

FIG. 6. Temperature dependence of the magnetic intensity measured at a Bragg angle of 23.2°, where the circles and triangles mark, respectively, the data taken without and with an analyzer-crystal. The ordering temperature for the Fe spins in FeOCl is $T_N \approx 80$ K.

$$S_{n1}=\begin{pmatrix} -\sin\alpha_n \\ 0 \\ \cos\alpha_n \end{pmatrix} \text{ and } S_{n2}=\begin{pmatrix} \cos(\alpha_n-\pi K) \\ 0 \\ \sin(\alpha_n-\pi K) \end{pmatrix}$$

fits the observations. Both of these spin vectors do not carry a component along the *b*-axis direction, showing that the moment lies in the *a*-*c* plane. Figure 5 shows the proposed magnetic structure at low temperature for the Fe spins in the *a*-*c* plane. The moment directions for the neighboring spins along the *a*-axis direction are $2\times360°/7\approx102.85°$ apart, accounting for the $k_x=2/7$ obtained for the modulation along the *a*-axis direction. Unfortunately, the relative orientations of the moments between the neighboring layers (along the *c*-axis direction) within each bilayer cannot be uniquely determined from the intensity calculations, as has been pointed out by Adam and Buisson.[14] The relative orientations of these moments shown in Fig. 5 are arbitrarily chosen. Nevertheless, the moments between the neighboring bilayers are antiferromagnetically coupled, as shown in Fig. 5. Along the *b*-axis direction, the neighboring spins are antiparallel (not shown). Comparisons between the observed and calculated magnetic intensities are listed in Table II, where the factor of 1.57 (as discussed above) for the *c*-axis preferred orientation has been taken into account, and the intensities are normalized with respect to the isolated peak at 23.2°. Clearly, the agreement is excellent, showing that the proposed spin structure fits to the observations well.

The quite distinct spin configurations obtained for the Fe ions along the three crystallographic directions can be readily understood from the crystallographic anisotropy of the Fe and O ions. In edge-sharing $FeCl_2O_4$ octahedrons, the *d* orbitals of Fe^{3+} are split by the crystalline electrical field effect into e_g and half-filled t_{2g} orbitals, while O^{2-} occupies the filled *p* orbitals.[27,28] Two types of magnetic couplings between the Fe ions may then be anticipated, a ferromagnetic direct-exchange (FMDE) coupling between two neighboring Fe e_g orbitals, and an antiferromagnetic superexchange (AFMSE) coupling between two Fe half-filled t_{2g} orbitals mediated through the O *p* orbitals located between them.[29] Clearly, the coupling strength depends strongly on the geometry of the Fe-O-Fe bonding. A wider Fe-O-Fe bond angle gives rise to a stronger AFMSE interaction, while a shorter Fe-Fe separation results in a stronger FMDE interaction. Along the *b*-axis direction, a simple antiferromagnetic arrangement was observed, showing that the AFMSE coupling dominates the FMDE coupling. This behavior can be understood, since the Fe-O-Fe bond angle (~148.9°) is large and the Fe-Fe are well separated (~3.763 Å at 10 K) along this direction. Along the *a*-axis direction, on the other hand, the Fe-O-Fe bond angle is smaller (~103.5°) and has a shorter

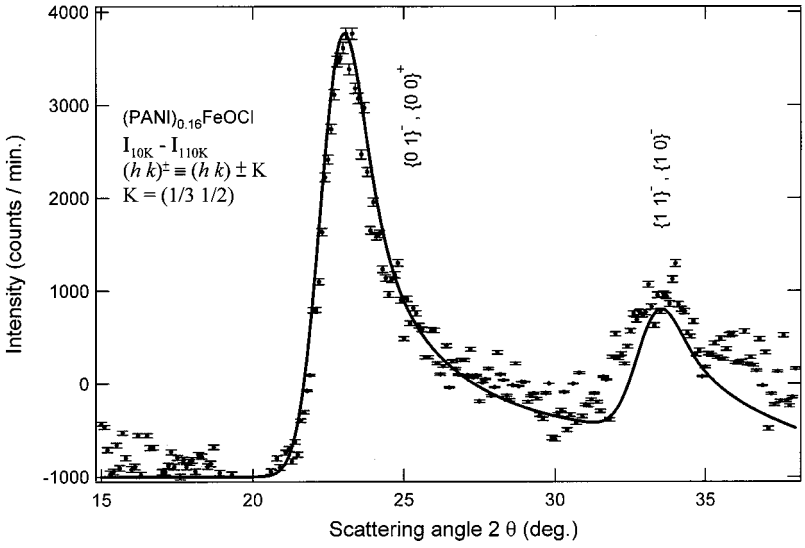

FIG. 7. Magnetic diffraction pattern of $(PANI)_{0.16}FeOCl$ obtained at 10 K, showing a standard coupled-bilayer Q2D scattering profile.

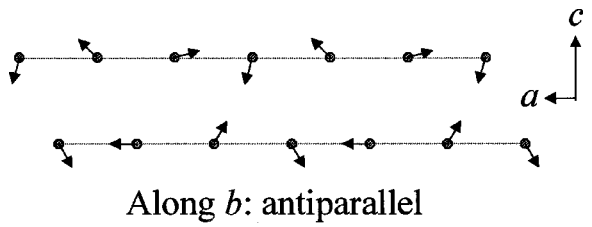

FIG. 8. Proposed magnetic structure for the Fe spins in $(PANI)_{0.16}FeOCl$ at low temperatures. The two neighboring Fe moments along the *a*-axis direction are 120° apart, whereas that along the *b* axis are antiparallel.

Fe-Fe separation (~3.290 Å at 10 K). A stronger FMDE interaction and a weaker AFMSE interaction hence result. Competition between these two types of couplings then gives rise to a noncollinear spin arrangement, so that the two neighboring moments are $2\times360°/7\approx102.85°$ apart. The coupling along the *c*-axis direction is crystallographically separated into intrabilayer and interbilayer interactions. The intrabilayer interaction is similar to that along the *a*-axis direction, but has a more compact Fe-O-Fe bonding, with a bond angle of ~99.6° and a Fe-Fe separation of ~3.092 Å at 10 K. A smaller angular separation between the two neighboring moments along the *a*-axis direction can be expected, but cannot be uniquely resolved from the present data. Most likely, the interbilayer coupling is dominated by the dipolar interaction, since the neighboring bilayers are bonded via a weak Van der Waals interaction, rendering the superexchange interaction insignificant.

Figure 6 shows the temperature dependence of the magnetic peak at $2\theta=23.2°$, where the circles and the triangles mark, respectively, the data taken without (energy-integrated) and with (elastic) an analyzer crystal. At low temperatures, there is essentially no difference between the data taken with or without an analyzer crystal, which reveals a typical order-parameter curve for polycrystalline samples. The ordering temperature of the Fe spins, as determined by the inflection point of the order-parameter curve, is $T_N\approx80$ K. Above T_N, the two curves are obviously different, indicating that there is a substantial contribution from dynamical spin fluctuations which exceeds the energy resolution of ~1 meV. By comparing the magnetic intensities to the nuclear ones, we obtained a saturated moment of $\langle\mu_Z\rangle=4.01(5)\mu_B$ for the Fe ions, which is in good agreement with the expected moment of $4.0\mu_B$.

B. $(PANI)_{0.16}FeOCl$

In Fig. 7, we show the magnetic diffraction pattern of $(PANI)_{0.16}FeOCl$ obtained at 10 K, where the diffraction pattern taken at 100 K, serving as the nonmagnetic background, has been subtracted. This pattern reveals peaks that developed as the temperature was reduced from 100 to 10 K, signifying the Fe spin ordering. As seen in Fig. 7, the observed magnetic reflections have a sharply rising leading edge followed by a trailing edge extending to large scattering angles. Such an asymmetric scattering profile with an oscillatory intensity is characteristic of coupled-bilayer Q2D behavior.[30–32] The solid curve shown in Fig. 7 is a fit of the data to the coupled-bilayer 2D magnetic scattering profile[32] convoluted with the Gaussian instrumental resolution function. Clearly, the fit is very good, showing that the observed pattern can be described well using the proposed bilayer profile. The magnetic peaks were identified as originating from the (1/3 1/2) rod of a coupled-bilayer spiral spin configuration shown in Fig. 8. Again, the relative orientations of the moments between the neighboring layers cannot be uniquely determined from the present data. Accordingly, the magnetic unit cell triples the nuclear one along the *a*-axis direction and doubles that along the *b*-axis direction, while no significant magnetic correlations between the neighboring bilayers were observed.

Evidently, the interbilayer couplings in $(PANI)_{0.16}FeOCl$ are interrupted by the appearance of polyaniline in the Van der Waals gaps that double the gap separation, rendering the dipolar interactions between the neighboring bilayers insignificant. The angular separation between the two neighboring Fe moments along the *a*-axis direction in $(PANI)_{0.16}FeOCl$ ($360°/3=120°$) is larger than that in FeOCl ($2\times360°/7\approx102.85°$), showing a stronger AFMSE interaction for the former than for the latter. This observation can be understood, since in $(PANI)_{0.16}FeOCl$ the *a*-axis Fe-O-Fe bond angle (~104.8°) is 1.3% wider and the Fe-Fe are 1.5%

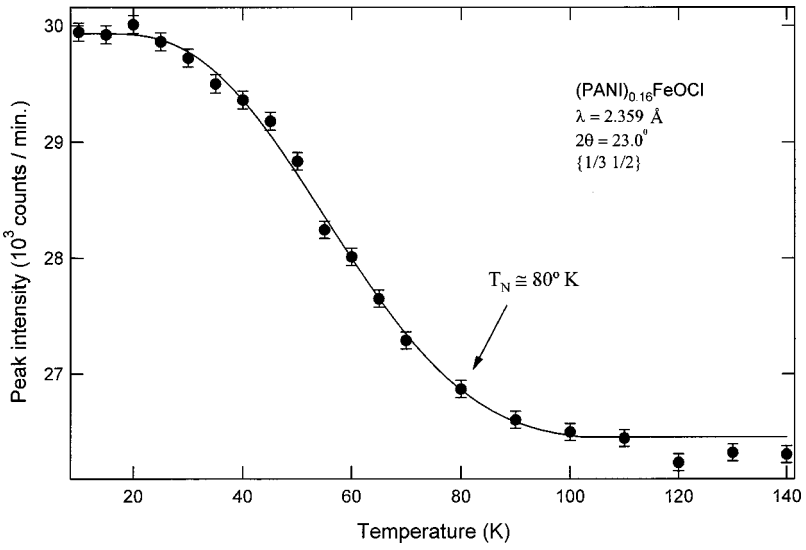

FIG. 9. Variation of the (1/3 1/2) peak intensity with temperature, showing a $T_N\approx80$ K for the Fe spins in $(PANI)_{0.16}FeOCl$.

further apart (~3.339 Å at 10 K), as compared to that in FeOCl. Apparently, the spin arrangement along the *b*-axis direction is not affected by the intercalation reaction that increases the Fe-O-Fe bond angle (~149.2°) by 0.2% and the Fe-Fe separation (~3.822 Å at 10 K) by 1.5%, along this axis direction. The ordering temperature, on the other hand, was not significantly affected by the appearance of polyaniline in the gaps, as seen in the temperature dependence of the (1/3 1/2) peak intensity, shown in Fig. 9, indicating a $T_N \approx 80$ K for the Fe spins in $(PANI)_{0.16}FeOCl$ as well. It is the intrabilayer couplings that determine the ordering temperature, as expected. The saturated moment obtained for the Fe ions in $(PANI)_{0.16}FeOCl$ is $3.98(7)\mu_B$, which is essentially the same value as obtained for the Fe ions in FeOCl.

IV. CONCLUSION

The crystal and magnetic structures of layered FeOCl have been investigated in detail. The iron-oxychloride FeOCl structure consists of Q2D charge-neutral $(Fe_2O_2Cl_2)_n$ lamellas linked via Van der Waals interactions. This Van der Waals gaped Q2D nature makes FeOCl a good host for intercalation reactions. The basic $(Fe_2O_2Cl_2)_n$ lamellas consisted of edge-sharing distorted $FeCl_2O_4$ octahedrons forming a bilayered anisotropic Fe-O-Fe network. A three-dimensional long-range ordering of the Fe spins in FeOCl develops below 80 K, where the moment becomes saturated at below ~20 K. Competition between the antiferromagnetic Fe-O-Fe superexchange coupling and the ferromagnetic Fe-Fe direct exchange coupling gives rise to a noncollinear magnetic structure for the Fe spins. The arrangement of the Fe moments is controlled by the Fe-O-Fe bond angle. An anisotropic Fe-O-Fe network results in different configurations for spins along the three crystallographic directions. Dipolar interactions, across the Van der Waals gaps, are also necessary for 3D long-range ordering to occur. This interbilayer interaction, however, becomes insignificant in $(PANI)_{0.16}FeOCl$, where a coupled-bilayer quasi-two-dimensional order of the Fe spins was observed. The existence of polyaniline in the gaps interrupts, rather than enhances, the magnetic interactions between the neighboring $(Fe_2O_2Cl_2)_n$ bilayers, indicating that there is no significant magnetic interaction between the polyaniline and the $(Fe_2O_2Cl_2)_n$ lamellas.

ACKNOWLEDGMENTS

This work at NCU was supported by the National Science Council of the Republic of China under Grant No. NSC 89-2112-M-008-051.

[1] S. M. Kauzlarich, J. L. Stanton, J. Faber, Jr., and B. A. Averill, J. Am. Chem. Soc. **108**, 7946 (1986).
[2] R. S. Bannwart, J. E. Phillips, and R. H. Herber, J. Solid State Chem. **71**, 540 (1987).
[3] S. M. Kauzlarich, B. K. Teo, B. A. Averill, Inorg. Chem. **25**, 1209 (1986).
[4] M. G. Kanatzidis, L. M. Tonge, T. J. Marks, H. O. Marcy, and C. R. Kanaewurf, J. Am. Chem. Soc. **109**, 3797 (1987).
[5] M. G. Kanatzidis, C.-G. Wu, H. O. Marcy, D. C. DeGroot, and C. R. Kannewurf, Adv. Mater. **2**, 364 (1990).
[6] C.-G. Wu, D. C. DeGroot, H. O. Marcy, J. L. Schindler, C. R. Kannewurf, T. Bakas, V. Papaefthymiou, W. Hirpo, J. P. Yesinowski, Y.-J. Liu, and M. G. Kanatzidis, J. Am. Chem. Soc. **117**, 9229 (1995).
[7] Z. Takehara, K. Kanamura, N. Imanishi, and C. Zhen, Bull. Chem. Soc. Jpn. **62**, 1567 (1989).
[8] T. R. Halbert and J. Scanlon, Mater. Res. Bull. **14**, 415 (1979).
[9] F. Kanawaru, and M. Koizumi, Jpn. J. Appl. Phys., Part 1 **13**, 1319 (1974).
[10] Z. Takehara, H. Sakaebe, and K. Kanamura, J. Power Sources **43–44**, 627 (1993).
[11] H. Sakaebe, S. Higushi, K. Kanamura, and H. Fujimoto, J. Power Sources **56**, 165 (1995).
[12] S. Kikkawa, F. Kanawaru, and M. Koizumii, Bull. Chem. Soc. Jpn. **52**, 963 (1979).
[13] K. Prassides, C. J. Bell, A. J. Dianoux, C.-G. Wu, and M. G. Kanatzidis, Physica B **180&181**, 668 (1992).
[14] A. Adam and G. Buisson, Phys. Status Solidi A **30**, 323 (1975).
[15] M. R. Halbert, in *Introduction Chemistry*, edited by M. S. Whittingham and A. J. Jacobson (Academic, New York, 1982), p. 377.
[16] H. M. Rietveld, J. Appl. Crystallogr. **2**, 65 (1969).
[17] *The Rietveld Method*, edited by R. A. Young (Oxford University Press, New York, 1993).
[18] A. C. Larson and R. B. Von Dreele, Los Alamos National Laboratory, Report No. LA-UR-86-748, 1990 (unpublished).
[19] J. Rouxel and P. Palvadeau, Rev. Chim. Miner. **19**, 317 (1982).
[20] J.-H. Choy, J.-B. Yoon, D.-K. Kim, and S.-H. Hwang, Inorg. Chem. **34**, 6524 (1995).
[21] W. A. Dollase, J. Appl. Crystallogr. **19**, 267 (1986).
[22] A. March, Z. Kristallogr. **81**, 285 (1932).
[23] M. D. Lind, Acta Crystallogr., Sect. B: Struct. Crystallogr. Cryst. Chem. **20**, 1058 (1970).
[24] G. E. Bacon, *Neutron Diffraction*, 3rd ed. (Clarendon, Oxford, 1975).
[25] O. V. Kovalev, *Irreducible Representations of the Space Groups* (Gordon and Breach, New York, 1965).
[26] Yu. A. Izyumov, V. E. Zaish, R. P. Ozerov, and Joachim Büchner, *Neutron Diffraction of Magnetic Materials* (Consultants Bureau, New York, 1991).
[27] J. B. Goodenough, Phys. Rev. **117**, 1442 (1960).
[28] E. O. Wollan, Phys. Rev. **117**, 387 (1960).
[29] P. W. Anderson, Phys. Rev. **79**, 350 (1950).
[30] B. E. Warren, Phys. Rev. **59**, 693 (1941).
[31] J. K. Kjems, L. Passell, H. Taub, J. G. Dash, and A. D. Novaco, Phys. Rev. B **13**, 1446 (1976).
[32] Details can be found in H. Zhang, J. W. Lynn, and D. E. Morris, Phys. Rev. B **45**, 10 022 (1992).